Front. Optoelectron. China 2008, 1(3–4): 263–267
DOI 10.1007/s12200-008-0068-3

RESEARCH ARTICLE

A genetic algorithm used in a 61-element adaptive optical system

Ping YANG (✉)[1,2], Bing XU[1], Wenhan JIANG[1], Shanqiu CHEN[1]

1 Institute of Optics and Electronics, Chinese Academy of Sciences, Chendu 610209, China
2 Graduate School of Chinese Academy of Sciences, Beijing 100039, China

Abstract To correct the phase aberrations in a wavefront, a wavefront sensorless adaptive optical (AO) system is set up. A real-number encoding Gaussian mutation genetic algorithm (GA) that is adopted to control a 61-element deformable mirror (DM) is presented. This GA uses the light intensity behind a pinhole on the focal plane as the objective function to optimize, and therefore to omit the procedure of measuring the phase aberrations in the laser wavefront by a wavefront sensor. Phase aberrations generated by the DM are brought to an ideal incident wavefront. Several correction simulations have been accomplished. The simulation results show that the genetic algorithm is capable of finding the optimum DM shape to correct the phase aberrations. After the phase aberrations of the wavefront have been corrected by GA, the peak light intensity on the focal plane can be improved at most by a factor of 30, and the encircled energy Strehl ratio can be increased ultimately to 0.96 from 0.032. It is also found that the convergence and stability of the 61 voltages on the DM is quite well. The simulation results prove that the genetic algorithm can be used in AO systems effectively.

Keywords adaptive optics, peak intensity, genetic algorithm, deformable mirror, Zernike polynomial

1 Introduction

When a conventional adaptive optical (AO) system is adopted for phase aberrations correction, more often than not, the necessary process is to measure the wavefront phase aberrations with a wavefront sensor and then using a wavefront corrector to compensate them based on some control algorithms [1–4], therefore, the wavefront measurement process is necessary in such a system. However, there are some special AO systems that detect the image quality affected by phase aberration in wavefront rather than measure the phase aberration itself. The image quality is then regarded as a sharpness function. When wavefront aberration is corrected completely, the sharpness function reaches its optimum value. More than 20 years ago, the LF12 laser system built in China adopted this AO system [5]. In recent years, these AO systems have been successfully used in many fields, such as correcting the phase aberrations in confocal microscopes and optimizing the coupling efficiency of single mode fiber and so on [6,7]. Generally, the hill climbing (HC) algorithm is one of the most common control algorithms used in these AO systems in the past few years. However, the HC algorithm often falls into local optimum in many applications. As a result, it is gradually replaced by some global algorithms. Genetic algorithm (GA) is a powerful global search algorithm, and theoretical research proves that GA can find the optimum value of problems as long as proper operating parameters are chosen. Based on the basic principle of GA, a real number encoding Gaussian mutation GA which is adopted to control a 61-element deformable mirror (DM) is presented in this paper. Some simulations have been done, moreover, the correction performance and the convergence ability of GA have also been researched.

2 Wavefront sensorless AO system based on GA

2.1 A typical wavefront sensorless AO system

Figure 1 shows a typical wavefront sensorless AO system. The laser wavefront with phase aberrations is incident on the DM. After being reflected by the DM, it is focused on the focal plane by a lens. A photoelectric detector is placed behind a small pinhole on the focal plane, and used to

Translated and revised from *Acta Optica Sinica*, 2007, 27(9): 1628–1632 [译自:光学学报]

E-mail: pingyang2516@163.com

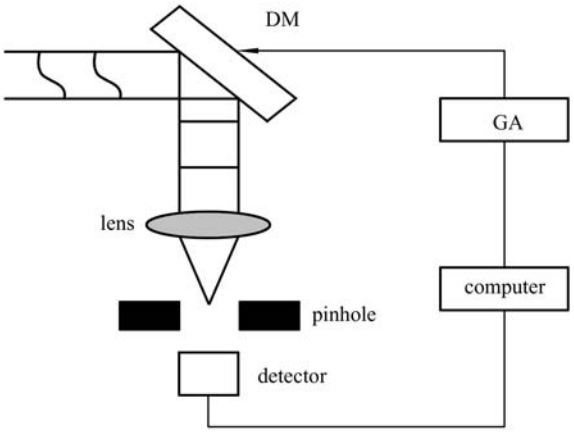

Fig. 1 Schematic of AO system without wavefront sensor

detect the light intensity of the laser beam that passes through the pinhole. Take the light intensity as the fitness function of GA for optimization, the DM changes its shape to maximize the fitness function and compensate the phase aberrations under the control of GA.

Supposing that the incident wavefront is $W_1(r, \theta)$ and the wavefront generated by DM is $W_2(r, \theta)$, r, θ are the variables in the polar coordinate respectively. To simplify the calculation, the radius of the object plane is normalized to 1. According to the theory of Fourier diffraction, the light intensity on the detector can be expressed as

$$F = I_0 \left| \int_0^{2\pi} \int_0^1 \frac{1}{\pi} \exp(\mathrm{j}W_1(r,\theta) - \mathrm{j}W_2(r,\theta)) r \mathrm{d}r \mathrm{d}\theta \right|^2, \quad (1)$$

where I_0 is a value proportional to the power of the laser beam, $\mathrm{j} = \sqrt{-1}$.

If $A = (A_1, A_2, \ldots, A_k, \ldots, A_n)$ are the Zernike coefficients of the wavefront to compensate and $B = (B_1, B_2, \ldots, B_k, \ldots, B_n)$ are the Zernike coefficients of the wavefront generated by DM, then

$$W_1(r,\theta) = AZ_k(r,\theta), \quad (2)$$

$$W_2(r,\theta) = BZ_k(r,\theta). \quad (3)$$

Let $C = A - B$, and then Eq. (1) can be rewritten as

$$F(C) = I_0 \left| \int_0^{2\pi} \int_0^1 \frac{1}{\pi} \exp\left(\mathrm{j} \sum_{k=1}^{n} c_k Z_k(r,\theta) \right) r \mathrm{d}r \mathrm{d}\theta \right|^2. \quad (4)$$

Because of the orthogonal of Zernike polynomial, when $|C|$ is small, Eq. (4) can be described as

$$\begin{aligned} F(C) &= I_0 \exp(\mathrm{j}|C|) \approx I_0 (1 + |C|)^2 \\ &\approx I_0 \left(1 + 2\mathrm{j}|C| - |C^2|\right) \approx I_0 \left(1 - |C|^2\right). \end{aligned} \quad (5)$$

What we can get from Eq. (5) is that when the phase aberrations are corrected well, C is very small, and $F(C)$ is very large. When the phase aberrations are compensated completely, $|C| = 0$ and $F(C)$ reaches its maximum.

2.2 GA and its application in a 61-element AO system

GA is a stochastic parallel algorithm based on natural selection and biological genetics. It is often used to search the global optimum value of some multi-object problems [8]. Figure 2 is the flowchart of GA, and the main steps of running this algorithm are as follows: 1) create the initial population by generating a group of individuals; 2) encode individuals; 3) calculate the fitness value of every individual; 4) selection operation; 5) crossover and mutation operation; 6) evaluate the terminate criterion. Each individual in the population corresponds to a possible solution of an actual problem to solve. Before evaluating the fitness value, individuals are encoded to form a group of chromosomes. Fitness value is the evaluation of the chromosome to the actual solution; the better the fitness value, the more chances the chromosome will survive and enter the succeeding operations. After executing the six steps mentioned above, GA will generate a new population called a new generation. GA executes six steps again and again until the terminate criterion is satisfied.

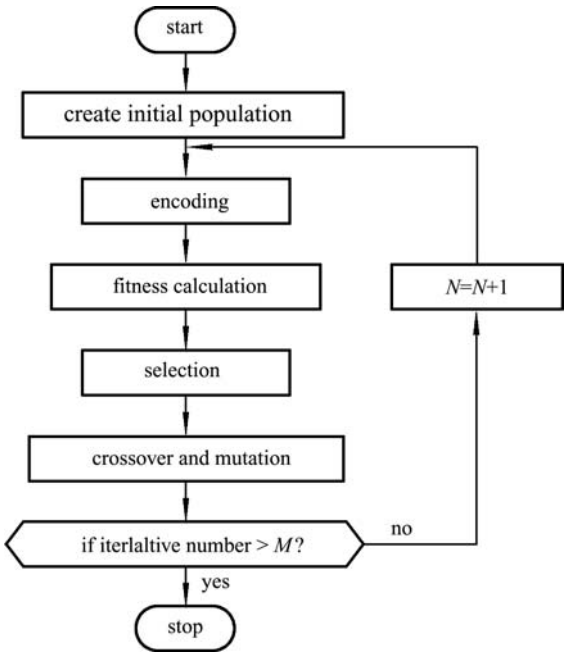

Fig. 2 Flowchart of GA

The configuration of the 61-element piezo-electric DM is shown in Fig. 3 and each black spot represents an actuator. Since the voltages that can be applied to 61 actuators on the DM are in the range of [−200 V, 200 V], if the updating step of voltages is 1 V, the 61 actuators can generate 400^{61} (10^{160}) different voltage groups; every group corresponds to a DM surface. Our purpose is to

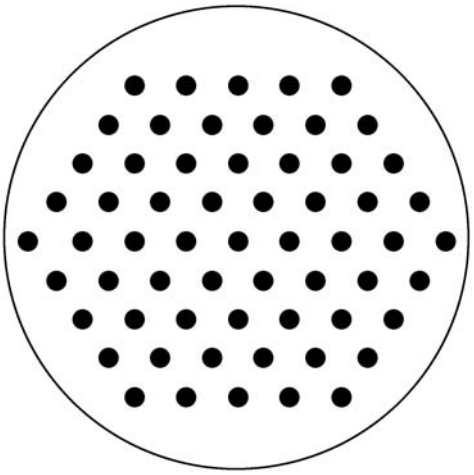

Fig. 3 Configuration of the 61-element DM

make the DM find the optimum surface shape from 10^{160} shapes for correct phase aberrations under the control of GA. The realization of this GA in a 61-element AO system will be described in detail as follows: a) Creating a population which consists of a group of individuals, in which each individual represents a DM surface shape and can be encoded with real-number encoding strategy. As to real-number encoding, use 61 voltages to form a chromosome $U=[V_1,V_2,\ldots,V_k,\ldots,V_{61}]$, whereas V_k $(k=1,2\ldots,61)$ is considered as a gene. b) Calculate the fitness value after the encoding is finished. What can be known from Sect. 2.1 is that taking the light intensity after the pinhole in the focal plane as the fitness function is reasonable, thus, $F(C)$, described in Eq. (5) is adopted as the fitness function. c) After the fitness calculation, GA will execute the selection operation, and in this paper, the roulette selection operation is adopted. The best individual, corresponding to the best fitness value of each generation, is reserved directly to the next generation, and the remaining individuals will join in the normal genetic operations. Assume that the population includes M individuals, the fitness value of the kth individual is $F_k(C)$, then P_k, the probability of the kth individual being selected is

$$P_k=\frac{F_k(C)}{\sum_{i=1}^{M}F_i(C)} \quad (k=1,2,\ldots,M). \tag{6}$$

The larger the P_k is, the larger the chance that the kth individual will be selected. d) The next steps are to crossover the selected individuals and mutate them respectively according to a crossover rate P_c and a mutation rate P_m. According to the theory of GA, the crossover operation and mutation operation that will affect the global and local search ability of GA, respectively, are two key operations. Thus, it is important to select the proper crossover operator and mutation operator. The uniform arithmetical crossover operator and Gaussian mutation operator are adopted in the devices in this paper. The crossover and mutation method are based on a simple and elegant idea described below.

Assume that the two individuals selected for crossover are Y_M^t, Y_N^t, and after the crossover operation, the new individuals Y_M^{t+1} and Y_N^{t+1} can be described as below:

$$Y_M^{t+1}=AY_N^t+BY_M^t, \tag{7}$$

$$Y_N^{t+1}=AY_M^t+BY_N^t, \tag{8}$$

where $0<A<1$, $0<B<1$, $A+B=1$.

Gaussian mutation: using a stochastic number R which satisfies $N(\mu,\sigma^2)$ distribution to substitute a gene of the individual selected for mutation. R can be generated through a group of stochastic numbers that correspond to a uniform distribution. Assume that 20 numbers r_i $(i=1,2,\ldots,20)$ uniformly distribute in [0, 1], then R can be obtained as

$$R=\mu+\sigma\left(\sum_{i=1}^{20}r_i-10\right). \tag{9}$$

If V_k $(k=1,2,\ldots,61)$, which belongs to $\left[V_{\min}^k, V_{\max}^k\right]$, is the gene selected from a chromosome $U=[V_1,V_2,\ldots,V_k,\ldots,V_{61}]$ for mutation operation, and let

$$\mu=\frac{V_{\min}^k+V_{\max}^k}{2},$$

$$\sigma=\frac{V_{\max}^k-V_{\min}^k}{10},$$

then V_k', which is the new gene of $U'=[V_1, V_2,\ldots V_k',\ldots, V_{61}]$, can be described as

$$V_k'=\frac{V_{\min}^k+V_{\max}^k}{2}+\frac{V_{\max}^k-V_{\min}^k}{10}\left(\sum_{i=1}^{20}r_i-10\right). \tag{10}$$

3 Numerical simulation and analysis

According to the realization course of the GA in the 61-element AO system described in Sects. 2.1 and 2.2, some simulative work were accomplished. This GA takes total iterative times as the evaluate terminate criteria and the times are set to 1000. The phase aberration $W_1(r,\theta)$ that is generated by the 61-element DM [9–13] can be represented by the first 35 Zernike polynomial within the unit circle area. $W_1(r,\theta)$ is then focalized on the focal plane through fast Fourier transform (FFT). Set an aperture in the center of the focal plane and the size of this aperture is set as large as the Airy spot using a software. The

pure aperture of DM is 60, whereas the distance between the actuators is 16.4. The influence function of the actuators is

$$f(r) = \exp[\mathrm{In}(C_m)(|r|/r_0)^a], \tag{11}$$

where r_0 is the distance between the actuators [14], $a = 2$, $C_m = 0.25$.

$F(C)$, the total light intensity within the aperture is used as the object function to optimize. It is obvious that the larger the $F(C)$, the better the beam quality is. The size of the initial population of GA is set to 30, whereas the cross-over rate P_c and the mutation rate P_m of GA are set at 0.70 and 0.05 respectively. After 1000 times iterative calculation, the GA stops the calculation.

Figures 4(a) and 4(b) show that the near-field wavefront distributions before and after phase aberration are corrected respectively. We obtain that the peak to valley (PV) and root mean square (RMS) are reduced from 3.758λ ($\lambda = 632.8$ nm) and 0.245λ to 0.623λ and 0.062λ, respectively, after the correction.

Similarly, the comparisons of the far-field light intensity distribution are shown in Fig. 5. Figure 5(a) is the far-field intensity distribution with the phase aberration, while Fig. 5(b) demonstrates the correction case. We find that the peak intensity is improved by a factor of 30 after the phase aberration is compensated. Moreover, before the correction, the Strehl ratio is 0.032 while after the correction, the Strehl ratio is 0.96. Here, the encircled energy Strehl ratio is the ratio for the energy of an actual far-field light on focus plane to that of an ideal wavefront far-field light on focus plane in the range of Airy disc (r_0). Figure 6 shows the far-field encircled energy curves of the ideal wavefront, wavefront with the phase aberration and wavefront after the aberration correction. From this picture we can know that the correction performance is good and the total energy within the Airy spot area is 81% of the total energy of the focal plane. Figure 7 is a curve which represents the best normalized fitness of each generation during the searching process. What we get from Fig. 7 is that the fitness value increases monotonously with the iterative times and finally reaches a value close to the optimum value 1.

To evaluate the convergence performance of the 61 voltages on the DM, we make U_1, the voltages that generate the phase aberration subtract U_2, the voltages that compensate the phase aberration, and let $U_3 = U_1 - U_2$. The smaller the U_3 is, the better the convergence is. What can be seen from Fig. 8 is that U_3 gradually converges to a small steady range from a large unstable range ([−0.2, 0.2] from [−3, 3]) as the iterative time increases; therefore, the convergence of voltages is good.

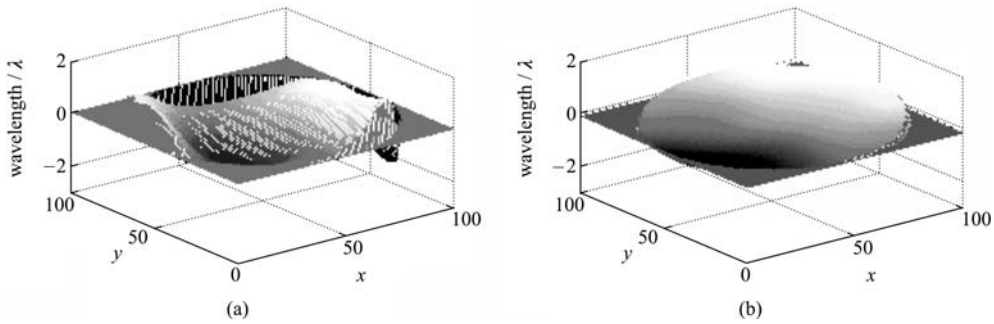

Fig. 4 Compensation performance of AO system controlled by GA. (a) Near-field phase distribution before correction (PV value is 3.758λ, RMS is 0.245λ); (b) near-field phase distribution after correction (PV value is 0.623λ, RMS is 0.062λ)

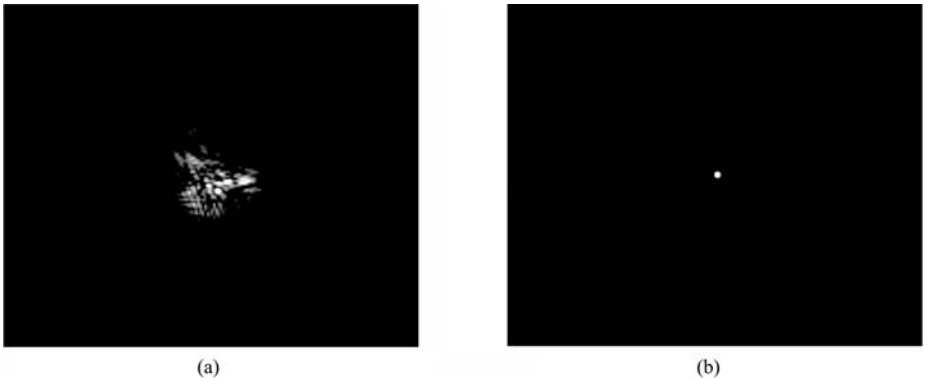

Fig. 5 Comparisons of far-field light intensity distribution. (a) Before correction (Strehl ratio is 0.032); (b) after correction (Strehl ratio is 0.96)

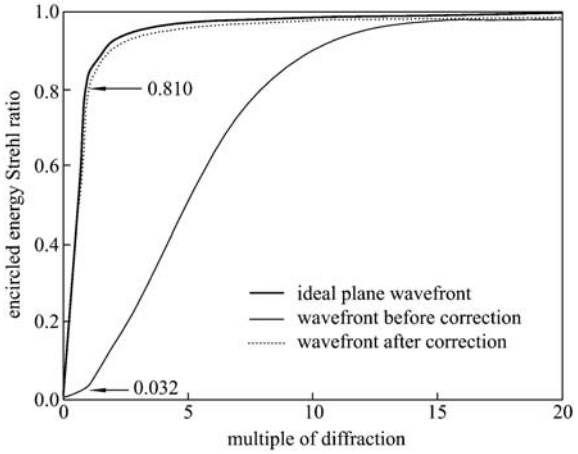

Fig. 6 Far-field encircled energy Strehl ratio curves

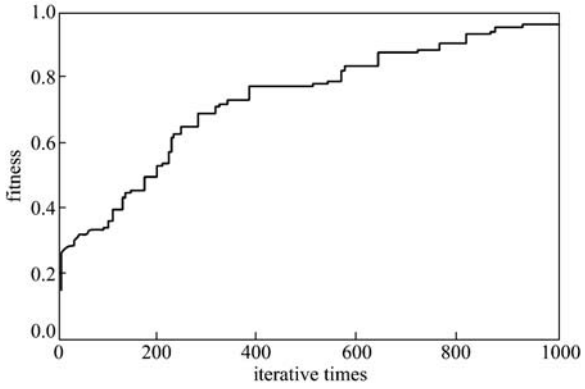

Fig. 7 Best normalized fitness of each generation during searching process

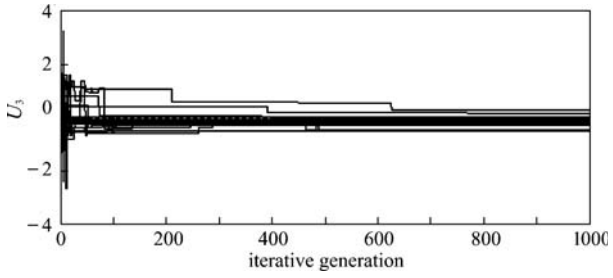

Fig. 8 Convergence of 61 voltages behind the DM

4 Conclusions

A Gaussian mutation GA is adopted in a 61-element wavefront sensorless AO system. The numerical simulation has been accomplished and the results prove the effectiveness of this algorithm: after 1000 times iterative calculation, the GA can find the optimum DM surface to compensate the phase aberration generated by the DM itself. The far-field peak intensity and Strehl ratio are both increased after the phase aberration is corrected. Since most of the run time is spent on the far-field light intensity calculation, as a result, the convergence speed is very slow. Fortunately, when the GA is used in the actual experiments, more often than not, the far-field light intensity is detected directly by a photoelectric detector which speeds the calculation of GA and saves the run time. However, to use this GA more effectively in an actual AO system, it is necessary to develop further researches, such as designing a more proper genetic operator and choosing a more reasonable fitness function.

References

1. Li Xinyang, Jiang Wenhan. Zernike modal wavefront reconstruction error of Hartmann-Shack wavefront sensor. Acta Optica Sinica, 2002, 22(10): 1236–1240 (in Chinese)
2. Hu Bian, Rao Changhui. The application of incremental Wiener filters in image deconvolution of wavefront sensoring. Acta Optica Sinica, 2004, 24(10): 1305–1309 (in Chinese)
3. Ling Ning, Zhang Yudong, Rao Xuejun, et al. A small adaptive optical imaging system for cells of living human retina. Acta Optica Sinica, 2004, 24(9): 1153–1158 (in Chinese)
4. Hou Jing, Jiang Wenhan, Ling Ning. Data fusion of the two Hartman-Shack wavefront sensors in the common path/common mode adaptive optics system. Acta Optica Sinica, 2004, 24(1): 131–136 (in Chinese)
5. Jiang Wenhan, Huang Shufu, Wu Xubin. Hill-climbing adaptive optics wavefront correction system. Chinese Journal of Lasers, 1988, 15(1): 17–21 (in Chinese)
6. Booth M J, Neil M A A, Juskaitis R, et al. Adaptive aberration correction in a confocal microscope. Proceedings of the National Academy of Sciences of the United States of America, 2002, 99(9): 5788–5792
7. Gonté F, Courteville A, Dändliker R. Optimization of single-mode fiber coupling efficiency with an adaptive membrane mirror. Optical Engineering, 2002, 41(5): 1073–1076
8. Goldberg D E. Genetic Algorithms in Search, Optimization and Machine Learning. Boston: Addison-Wesley Publishing Company, 1989, 25–50
9. Yang Ping, Hu Shijie, Yang Xiaodong, et al. Test and analysis of the time and space characteristics of phase aberration in a diode-side-pumped Nd:YAG laser. Proceedings of SPIE, 2005, 6018: 60180M
10. Lubeigt W, Valentine G, Girkin J, et al. Active transverse mode control and optimization of an all-solid-state laser using an intracavity adaptive-optic mirror. Optics Express, 2002, 10(13): 550–555
11. Burns D, Valentine G J, Lubeigt W, et al. Development of high average power picosecond laser systems. Proceedings of SPIE, 2002, 4629: 129–143
12. Albert O, Sherman L, Mourou G, et al. Smart microscope: an adaptive optics learning system for aberration correction in multiphoton confocal microscopy. Optics Letters, 2000, 25(1): 52–54
13. Marsh P N, Burns D, Girkin J M. Practical implementation of adaptive optics in multiphoton microscopy. Optics Express, 2003, 11(10): 1123–1130
14. Shao Li, Xian Hao. Influence of deformable mirror parameter variation on aberration correction for atmospheric turbulence. Opto-Electronic Engineering, 2004, 31(5): 7–10 (in Chinese)